JOURNAL OF MARITIME RESEARCH

Vol XXIII. No. II (2026) pp 257–272

ISSN: 1697-4840, www.jmr.unican.es

Impact of Jetty Extensions on Sediment Transport and Shoreline Stability: A Case Study of El-Manzala Lake, Port Said, Egypt

Mohamed M. Mirdan[1,*], Ehab R. Tolba[1], Elsayed M. Galal[1], Sherif Abdellah[1]

ARTICLE INFO

Article history:
Received 22 Aug 2025;
in revised form 09 Sep 2025;
accepted 28 Sep 2025.

Keywords:
Numerical Modeling, DHI-LITPACK, Shoreline Changes, Tidal Inlets, El-Manzala Lake.

ABSTRACT

This study examines the impacts of recent jetty extensions at the main tidal inlets of El-Manzala Lake on sediment transport and shoreline stability along the coastal stretch between Damietta and Port Said, with a focus on El-Gamil Beach. Utilizing the LITPACK numerical model, various scenarios were simulated to understand the hydrodynamic and sedimentary responses to these modifications over a 20-year period. The western jetty was extended seaward by 300 meters and the eastern jetty by 200 meters during 2019–2020. The findings reveal significant alterations in sediment dynamics, with notable erosion on the downdrift side and accretion on the updrift side of the inlets. Among the scenarios evaluated, the construction of emerging breakwaters and the implementation of sand nourishment emerged as the most effective strategies for mitigating erosion and stabilizing the shoreline. Specifically, sand nourishment demonstrated a balanced approach, leveraging natural processes to counteract erosion with minimal environmental impact. The study underscores the importance of integrating both engineering and environmental considerations in coastal management practices. Continuous monitoring and adaptive management are essential to address the dynamic nature of coastal systems. Future research should focus on long-term monitoring and the potential impacts of climate change on coastal erosion and sediment transport patterns. This research contributes valuable insights into the sustainable management of coastal regions, emphasizing the critical role of tailored interventions in preserving the ecological and economic integrity of coastal landscapes.

1. Introduction.

Tidal inlets are crucial openings in coastal barriers that facilitate the exchange of water between larger water bodies and smaller, more contained environments such as natural and artificial lakes, lagoons, marshes, and tidal creek systems (FitzGerald and Miner, 2021). These inlets are subject to varying currents and the ebb and flood of tides, significantly influencing the sedimentary architecture of shorelines (Gong and Burningham, 2024). At the mouths of lakes, coastal sediments are distributed through processes of erosion, trapping, and redistribution, shaping the coastal landscape (Beck et al., 2020). Managing these dynamic features presents significant engineering and environmental challenges, especially in regions with high economic and ecological value (Oyedotun and Nedd, 2023).

The coastal stretch between Damietta and Port Said, a jewel in Egypt's crown, is a testament to the intricate balance between nature and human development (Tharwat Sarhan et al., 2022). This region is adorned with significant investments such as the Egyptian propylene polypropylene company, United Gas Derivatives Company (UGDC), the Zohr gas field, and residential and leisure complexes like El-Fayros village, Porto-Said resort spa, and Tower-Bay beach, faces the Mediterranean Sea. In stark contrast, the Port Said International Airport and Astoumn El-Gamil National Park lie on the opposite side, highlighting the area's diverse utilization (A. T. Sarhan et al., 2022) In this region, protective jetties have been constructed around the main

[1]Port Said University, Faculty of Engineering, Civil Engineering Department, Egypt.

[*]Corresponding author: Mohamed M. Mirdan. E-mail Address: mohamed.mirdan@eng.psu.edu.eg.

tidal inlets (A and B) of El-Manzala Lake, which extends into the Mediterranean Sea (see Fig. 1). During 2019-2020, the western jetty of the main tidal inlet (A) was extended seaward by 300 meters, while the eastern jetty was extended by 200 meters (Abd Ellah, 2022). These extensions are expected to impact the shoreline both updrift and downdrift of the main tidal inlet (A) due to sediment transport, wave diffraction, and other factors influenced by climatic changes. Additionally, the water currents resulting from the main tidal inlet of El-Manzala Lake transport sediment to and from the lake to the Mediterranean Sea, further complicating the hydrodynamic processes around the tidal inlets (Elshemy, 2017).

The study of tidal inlets and their impact on coastal sediment dynamics has been extensively explored globally. Classic studies by (Bruun, 1966; Escoffier, 1940) laid the groundwork for understanding the equilibrium of tidal inlets and their response to external forces such as sediment supply and wave action. More recent studies have focused on the complex interactions between tidal currents, wave energy, and coastal structures, highlighting the role of jetties in altering natural sediment transport processes as (Chan, 2024; FitzGerald and Miner, 2021; Hanegan et al., 2023; Khan et al., 2023; Mandal and Chaudhuri, 2021).

In the context of the Egyptian coast, research has primarily concentrated on the Nile Delta, where significant anthropogenic activities have altered coastal dynamics. Studies by (Ali W et al., 2017; El Banna and Hereher, 2009; Iskander, 2020; Mirdan et al., 2023; Nassar et al., 2018a; Radwan et al., 2021; A. T. Sarhan et al., 2022; Sarhan et al., 2020, 2020; Shaltout et al., 2015; Shaltout and Tonbol, 2011; Tharwat Sarhan et al., 2022)have documented the impact of coastal structures, such as jetties and groins, on shoreline stability and sediment distribution along the Mediterranean coast of Egypt. These studies emphasize the importance of understanding local hydrodynamic conditions and sediment transport patterns to effectively manage and mitigate coastal erosion. However, despite the extensive research on the Nile Delta and the broader Egyptian coast and the economic and ecological significance of the coastline between Damietta and Port Said, there is a noticeable gap in studies that specifically address the impacts of recent jetty extensions on sediment transport and shoreline stability in the region between Damietta and Port Said. This gap is particularly evident when considering the recent modifications to the jetties at El-Manzala Lake's main tidal inlet. The specific hydrodynamic and sedimentary responses to these extensions remain underexplored, leaving a critical knowledge gap that this study aims to fill. This paper aims to bridge this gap by examining the recent jetty modifications at El-Manzala Lake and their implications. It investigates the effects of the recent jetty extensions at the main tidal inlets of El-Manzala Lake on sediment transport and shoreline changes. By employing numerical modeling and field data analysis, we seek to understand the interactions between coastal structures and natural processes in this highly dynamic environment.

2. Regional Setting.

The coastal study zone stretches from latitudes 31°16'10" to 31°19'48" N and longitudes 32°09'05" to 32°15'18" E, as shown in Fig. 1. This area is an important area in the Egyptian Mediterranean coasts, situated to the west of the town of Port Said. It forms the northeast side of the El-Manzala Lake, which is one of the largest and most important coast's lagoons in Egypt. This lagoon serves as an interface between freshwater and brackish systems and opens directly to the Mediterranean Sea. The area is known for its diverse flora and fauna as well as its significant economic impact on the local and national level through fishing, farming, and tourism. This coastal belt has a rather active geomorphology that is constantly impacted by erosion and accretion processes of different magnitudes caused by various factors; these factors include natural processes like waves, sediment movements and tidal changes to manmade factors such as construction and damming. Such a context has led to the establishment of an extremely fragile terrain in which different parts of the coastline are in a state of active erosion, whereas some areas accumulate large quantities of sediment. There is notable environmental, social, and economic relevance for the study area. The region is also inhabited by humans who practice agriculture around the rich soils of El Manzala Lake and fisheries based around the lagoon's waters. Other small settlements and communities along the shoreline also use these resources as medicines and for trade. These activities, however, are being increasingly endangered by the adverse effects of environmental hazards such as coastal erosion, sea level rise, saltwater intrusion and climate change.

In addition, the geographical location of the study area relative to Port Said, which is a major metropolitan and industrial city, is also a source of complexities. The coastal infrastructure and shipping activities that Port Said engages in, as well as the urban expansion, create stress on the natural coastal processes. This highlights the demand for integrated and robust coastal management that indeed exists to address pollution and develop without harming the environment.

Due to the location of the region, its environmental importance and the threats of various risks, this area is a good case study for assessing the interaction between physical geographical features and alien impacts as well as climatic changes in the Mediterranean environment (Abd-Ellatif et al., 2024).

Between 2019 and 2022, the coastal zone located west of Port Said, concerning the geographical view, changed greatly as a result of a combination of natural and human activities, as shown in Fig. 2. Assessing shoreline erosion along the blended shoreline due to sediment processes, wave actions, and manmade structures (Morsy et al., 2022).

The areas east of the coastal protective structures, especially the jetties and the breakwaters at the tidal inlets Damietta, and Port Said, experienced deep sedimentation, which widened the beach profile during this period. On the other hand, the eastern side of such structures suffered from intense erosion that aggravated the shoreline retreat. This scour–fill imbalance is caused by these coastal structures cutting off the shoreline sediment system. Moreover, shifts in the prevailing winter climate

Figure 1: The study area location.

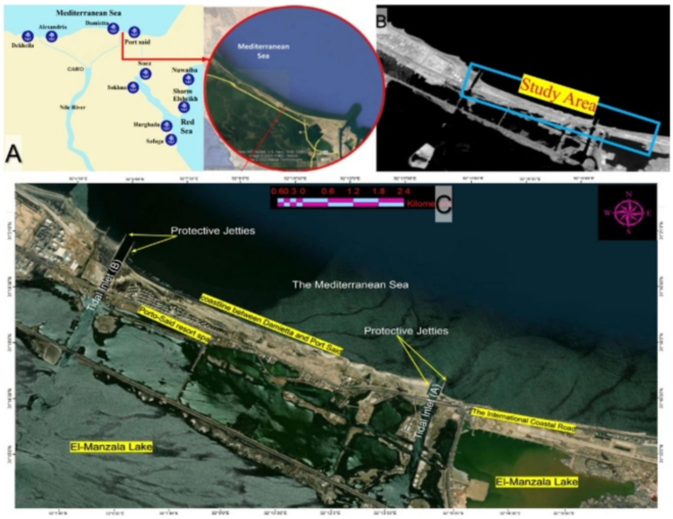

Source: Authors.

patterns have intensified storm activity and the erosive potential of coastal zones in the area, causing further coastal recession in agricultural and fishing areas. Coastal measures, which include protection works in the form of groins and jetties, which are affected by island mass, development of some areas, and loss of some have been implemented with mixed success (ElKotby et al., 2023).

A dynamic and complex interaction between hydrodynamic and sedimentary processes characterizes this region. The lake's tidal inlets (Bogaz El-Gamil), particularly at Damietta and Port Said, play a crucial role in regulating water exchange between the lake and the sea (A. Sarhan et al., 2022). The coastal stretch between Damietta and Port Said is a highly active coastline, prone to significant morphological changes due to both natural processes and anthropogenic interventions. The construction of jetties and breakwaters at the tidal inlets of Damietta and Port Said has significantly altered the coastal dynamics. These structures were initially built to stabilize the inlets and protect the adjacent shorelines from erosion.
However, they have also contributed to the interruption of the natural sediment transport, leading to accretion on the updrift sides and erosion on the downdrift sides of the structures (El-Asmar and Taha, 2022). The coastal stretch immediately adjacent to these inlets is an open coast, which experiences a net sediment transport predominantly towards the east due to the prevailing wave and current patterns. This sediment transport has been estimated to be approximately 0.50×10^5 to 1.00×10^5 m^3/year, resulting in the gradual accumulation of sediments along the eastern side of the jetties, while the western side continues to erode (Redwan and Elhaddad, 2022).

To mitigate the ongoing erosion and protect the shoreline, a series of coastal protection measures have been proposed and implemented in various stages. These include the extension of jetties and the construction of groins along the coast. The effectiveness of these measures, however, has been mixed, with some areas showing signs of stabilization, while others continue

Figure 2: Geographical Changes in the Coastal Zone West of Port Said (2019–2022).

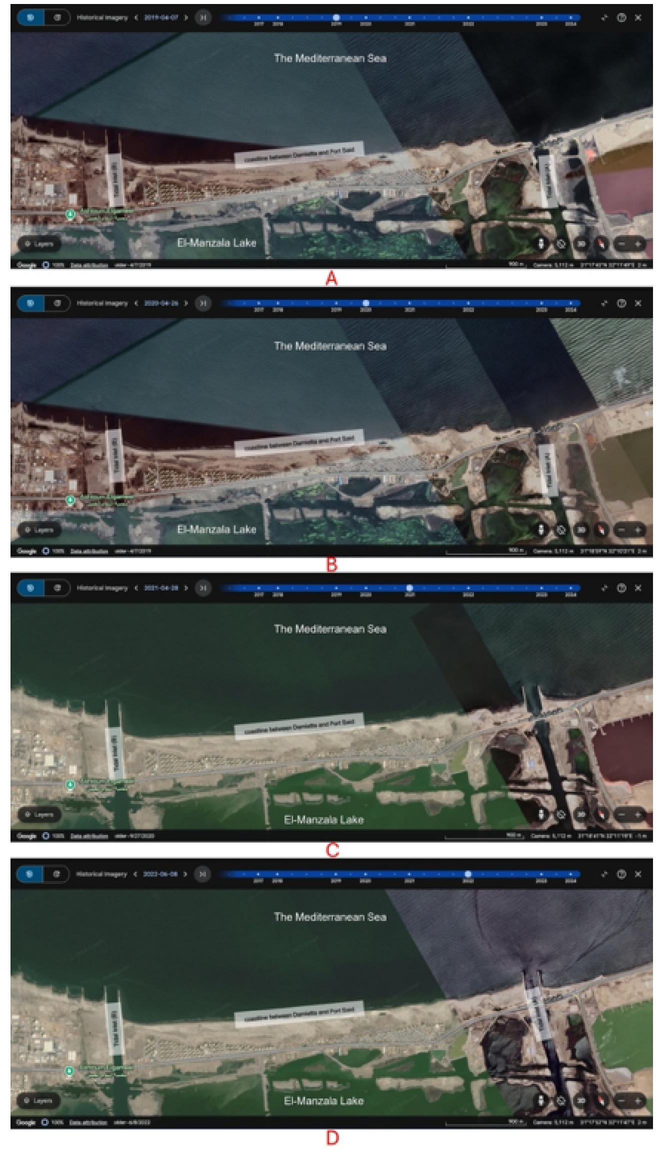

Source: Authors.

to experience significant erosion, particularly during the winter storm season (Ali and El-Magd, 2016). The tidal inlets themselves are critical for the exchange of water, nutrients, and sediments between El-Manzala Lake and the Mediterranean Sea. Any changes in their morphology, whether through natural processes or human intervention, have far-reaching implications for the ecological health of the lake and the stability of the surrounding coastline (Abdelaal et al., 2022).

3. Data and Methods.

The methodology followed these four stages: 1) Collection of data and information through literature review, field surveys, and online database; 2) Numerical modeling set-up and data processing; 3) Calibration and validation of the model and 4)

Model application under different scenarios.

3.1. Data.

3.1.1. Extracted shoreline positions.

Shoreline data spanning the years 2019 to 2022 (inclusive of 2019, 2020, 2021, and 2022) were derived from Landsat 8 (OLI/TIRS) (the Operational Land Imager/ the Thermal Infrared Sensor) satellite images. These images were processed and exported into the ArcGIS 10.5 software for coastline digitization. DSAS (Digital Shoreline Analysis System) was also employed to automate shoreline extraction. The shoreline positions extracted by (Mirdan et al., 2023), as shown in Fig. 3. His study focuses on two coastal areas that differ in terms of shoreline processes and the level of human activity. The first area stretches over the shoreline from the Port Said International Airport, up to the sea, and around the jetties of the El-Manzala Lake tidal inlet. This zone is characterized by high rates of accretion, especially at the airport (+10.30 m/yr) and along the left bank of El-Manzala Lake (+6.10 to +17.20 m/yr) due to the presence of groins, breakwaters, and jetties. On the other hand, it is reported that there was another wave of erosion (–27.20 m/yr) around tidal inlets that were infilled during the 2019–2020 period, limiting the normal sand movement along the beaches. The second area in progress roughly corresponds to the western direction from the groin system placed in the vicinity of the intake of El-Gamil up towards the areas in the vicinity of the Zohr gas field infrastructure. This zone is clearly and primarily an eroded zone with rates between –2.10 to –5.85 m/year, although there are, groins and jetties which were introduced in 2016 in some areas, where they were built to stop the erosion process, meaning a sovereign positive accretion rate to give way to the construction of a polypropylene factory on the shoreline (Mirdan et al., 2023).

Figure 3: Extracted shoreline positions at study area a) shorelines in years 2019, 2020, 2021, and 2022; b) Linear Regression Rate (LRR) at study area calculated by (Mirdan et al., 2023).

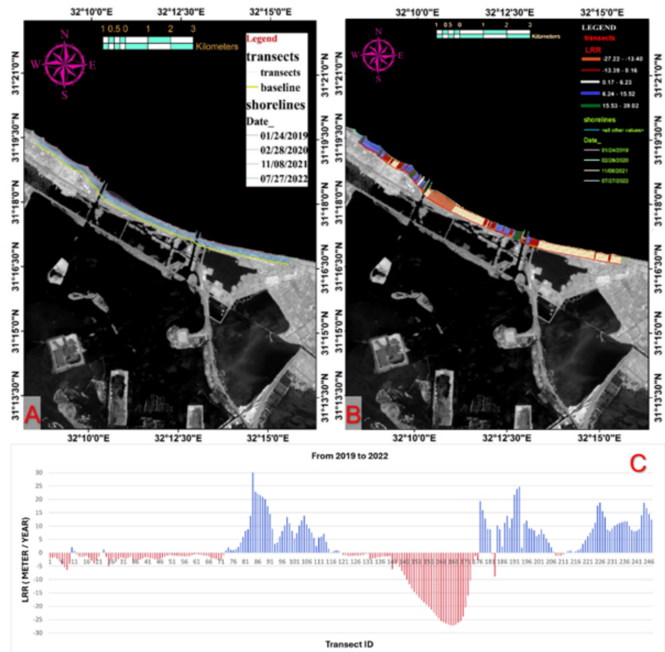

Source: Authors.

3.1.2. Bathymetry Map.

The bathymetric data, as shown in Fig. 4, used in this work was based on maps supplied by the Egyptian Shore Protection Authority Survey records dated December 2020 for Port Said. To get the needed information, these maps, which bore depth contours among other details, were scanned at high resolution. The bathymetry reveals maximum depth measurements covering the study area up to -13 meters which validates the relevance of this data to other related datasets.

The digitized form of the scanned documents was then brought into AutoCAD 2020 to begin the digitization process. The reference scanned maps corresponded with the reference odd points or grid lines shown on the original charts, maintaining that the maps' spatial relationships were positioned correctly when transferred to the electronic format. Bathymetric contours, depth points, and other objects of interest were on the subsequent stage traced within AutoCAD, and vectorized representations of the depth information were created.

For spatial precision and compatibility with other datasets, Civil 3D software was used to georeferenced the digitized contours. As part of the georeferencing process, maps were fitted or georeferenced to a known coordinate system with identifiable features, reference points, or grid systems shown on the source maps. The geo-referencing in this case was done to the Universal Transverse Mercator (UTM) coordinate system to facilitate other geospatial datasets.

After geo-referencing, the captured bathymetric features were transformed into an orderly data structure represented as (x, y, z), where x and y are spatial coordinates and z is the vertical dimension. This was done by taking particular areas where the depth perception curves were digitized and pulling points at a rigorously consistent distance. The resultant points were saved on a data file that could be used with LITPACK (Littoral Processes and Coastline Kinetics) for further investigation (Anton et al., 2017).

By visually examining the original map, cross-checking the digitization process was carried out to make sure the depth values and spatial correlations were accurate. To maintain the data's integrity and stop the underlying structure from deteriorating, all such mistakes were fixed. Through digitalization, multi-dimensional historical bathymetric data was transformed into a format suitable for spatial analysis and numerical modeling.

3.1.3. Sediment Data.

Each grid mark that defines the cross-shore profile necessitated sediment sample characterization. Sediment data were collected along 247 profiles, positioned approximately 50 meters apart, extending 12.35 kilometers from the coast. Field observations revealed non-cohesive sediment comprising sand-like particles near the prospective Port Said beach area. The sand size classification, detailed in Table 1, illustrates the sed-

Figure 4: Bathymetric Map of the study zone (Egyptian Shore Protection Authority).

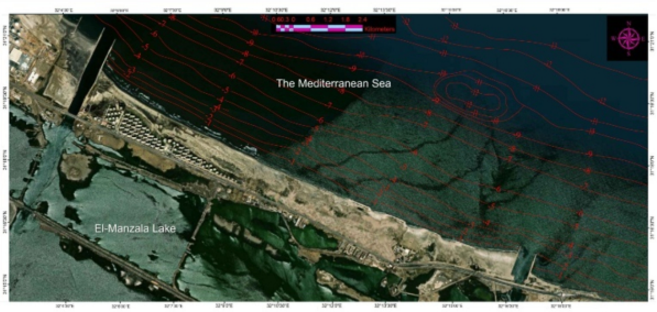

Source: Authors.

iment samples collected from upper shoreface (0-2 m), mid shoreface (2-5 m), and lower shoreface (5-10 m) depth intervals. Bottom d50 values for deeper zones were documented as 0.14 mm (fine sand) while coarser top regions reflected values of 1.19 mm. The height of the berms along these profiles ranged from 0.5 to 1 meter, with closure depth fluctuations between 2 to 4 meters (Holthuijsen, 2007).

The sediment characteristics and roughness values were derived from site measurements reported by (Nassar et al., 2018c, 2018b). These parameters informed the LITPACK 1D modeling conducted by (Sanhory et al., 2022), aimed at predicting potential alterations to the coastline. The analysis indicated no significant changes in the coastline's position, correlating with a decrease in particle size from an average of 0.40 mm to 0.14 mm. as detailed in Table. 1. Sediment transport capacity is determined using the LITPACK software (Naef et al., 2006).

The sediment profile across the study zone transitions from sandy beaches to muddy sand and fine sand in the offshore region, with muddy sediment predominating at depths greater than 10 meters (Eltokhi, 2008). Subsurface sediment layers within the Holocene delta plain display subsidence effects, becoming thinner or vanishing entirely westward, particularly near the Alexandria coastal plain (Dewidar and Frihy, 2003).

Table 1: Parameters for all cross-shore profiles' sediment.

Depth limits (m)	Fall Velocity (m/s)	Seabed roughness	d_{50} mm	Spreading factor $\sigma_g = \sqrt{1.50 d_{50}}$
From +3 To 0	0.11	0.015	0.901	1.103
From 0 To -3	0.081	0.011	0.512	0.627
From -3 To -5	0.024	0.006	0.245	0.3
From -5 To -7	0.004	0.006	0.095	0.116
From -7 To -9	.0001	0.006	0.009	0.011

Source: Nassar et al., 2018c, 2018b.

3.1.4. Wind Data.

To better understand the wind characteristics of direction, intensity, duration, and frequency, an analysis of archival wind records was undertaken. This study utilized wind and wave data for the period between January 1, 2019, and December 30, 2022, that were supplied by the Egyptian Navy's Division of Meteorological and Oceanographic Services in the Southeast Mediterranean Sea. These measurements were taken from S4DW buoys, the primary one being anchored off the northeast coast of Port Said, in 133 meters of water at 31°51'00.6"N and 32°25'19.2" E (Salah, 2024).

Reanalysis data or similar datasets available in large archives provide a better understanding of the local climate, and this helps to calibrate or confirm a given wind measurement technique. To calculate the specific locations of significant occurrences, we used very high-resolution historical wind data originating from reanalysis. The maps of prevalence zones were produced from the recorded data collected during the occurrence of important events. To ensure accuracy and consistency, several wind times were systematically selected within the observation area. In addition, we were able to locate centers of considerable activity with great precision because of the high detail of historical data. A calibrated anemometer was set up 10 meters above the ground and placed at a specific standard height to ensure greater reliability and accuracy of the results, and the wind data were collected systematically every 10 minutes.

Taking into account that such databases do exist, large-scale wind measurements can offer a much broader perspective rather than evaluations made at a singular wind site. Measurements of wind in different areas have an opportunity to complement each other more efficiently. Wind speed and wind direction do not stay stagnant and they tend to shift throughout different periods, thus spanning several decades. Due to this variability, a cross-sectional analysis is best suited as it helps dodge issues related to non-stationarity. This means that the analysis accounts for surfaces that shift significantly or surface winds that span across eras that do not share any correlation.

Such a detailed examination of historical wind patterns is essential for understanding their role in shaping coastal and environmental processes, including sediment transport and wave energy generation. Fig. 5 presents the wind rose, illustrating both the directional distribution and probability values for various wind speed intervals.

3.1.5. Wave Data.

The ERA5 reanalysis dataset, developed by the Copernicus Climate Change Service, was utilized to provide a comprehensive historical wave dataset for the study area. ERA5 offers global coverage of atmospheric and wave data, with hourly temporal resolution and a spatial resolution of approximately 31 km, spanning several decades from 1950 to the present. This extensive dataset ensures a robust statistical representation of the wave climate and serves as a reliable basis for the study of coastal dynamics.

Wave parameters, including significant wave heights (H_S), wave periods, wave frequencies and wave directions, were ex-

Figure 5: The wind rose in the study area.

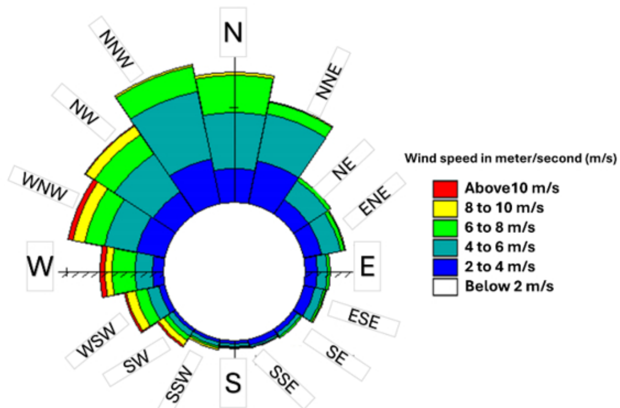

Source: Authors.

tracted from the ERA5 database at a specific offshore location in the Mediterranean Sea (latitude:32.0°N, longitude: 32.5°E), where the water depth is approximately 100 meters. These offshore wave conditions were subsequently propagated to the nearshore zone using the Simulating Waves Nearshore (SWAN) model, a third - generation spectral wave model designed for coastal and nearshore environments. SWAN accounts for key wave transformation processes, including refraction, shoaling, breaking, and diffraction, ensuring an accurate representation of wave behavior as waves travel from deep water to the coast. This method allowed for the characterization of the wave conditions impacting the nearshore areas of Port Said, Egypt. The significant wave heights for the nearshore surface waves ($H_{S'}$) off Port Said, Egypt, exhibited a range of 0.05 m to 2.36 m, with an average value of 0.51 m. The temporal distribution of these near-wave heights is depicted in Fig. 6, illustrating the variation in wave energy reaching the coast. While the figure focuses on significant wave height for clarity, the analysis also considered wave direction and frequency of events, which are critical for understanding coastal morpho dynamics. These additional parameters were incorporated into numerical modeling to ensure a comprehensive representation of wave dynamics.

The time series presented in Fig. 6, spans from 01-01-2019 to 01-12-2022, a period selected to align with recent coastal changes observed in the study area. However, to ensure a robust understanding of the average wave climate, a statistical analysis of the entire ERA5 dataset (1950–present) was conducted. This long-term analysis provided insights into climatic variability and trends, which were used to validate the representativeness of the shorter time series. The combination of long-term statistical analysis and recent time series data ensures that the study captures both historical trends and contemporary wave conditions.

By leveraging the ERA5 dataset, the study achieves a detailed representation of wave dynamics over a sufficiently long period, addressing the limitations of short-term datasets that may not capture climatic variability or long-term trends. However, it is important to note that the accuracy of the results depends on the fidelity of the ERA5 data and the wave transformation model. While no direct comparison with measured nearshore wave data was conducted in this study, the ERA5 dataset and the selected wave transformation model have been widely validated in previous studies, supporting their use in this context. This approach enhances the reliability of the input data used in numerical modeling and provides a solid foundation for both calibrating models and simulating future scenarios.

Incorporating high-quality historical wave data ensures a comprehensive understanding of the wave regime and its influence on coastal morpho dynamics, facilitating more robust conclusions regarding shoreline stability and sediment transport processes.

Figure 6: Coastal hydrodynamics in the El-Manzala Lagoon: wave height and period.

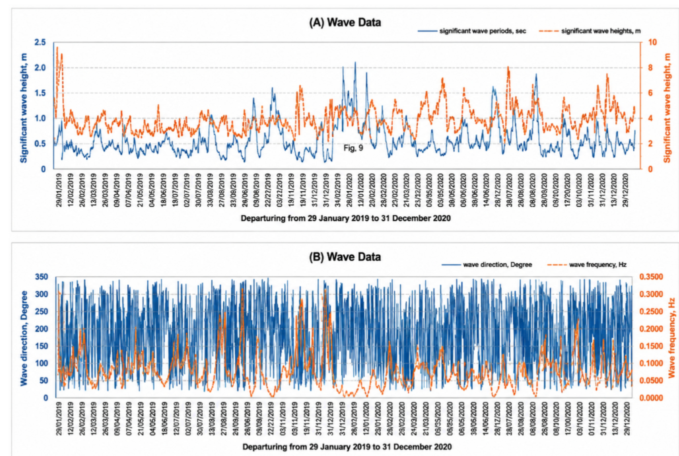

Source: Authors.

3.1.6. Tidal Data.

An hourly sea-level dataset was collected from the Port Said shoreline by (Halawany et al., 2022). The tidal regime ratio was calculated using the Form Factor (FF) equation, yielding a value of 0.21, which indicates a semidiurnal tidal domain in the area. Tidal datum levels were established relative to the Egyptian Surveying Authority (ESA) zero datum, as provided by the Suez Canal Research Institute (SCRI). Additionally, tidal levels were calculated using MATLAB, in accordance with the latest definitions of the Lowest Astronomical Tide (LAT) and Highest Astronomical Tide (HAT) as recognized by the International Hydrographic Organization (IHO). The analysis revealed that the ranges between the highest and lowest tidal expressions, such as Mean High-Water Springs (MHWS) & Mean Low Water Springs (MLWS), Mean High Water Neaps (MHWN) & Mean Low Water Neaps (MLWN), Highest High-Water Level (HHWL) & Lowest Low Water Level (LLWL), and HAT & LAT, were 0.368 m, 0.096 m, 0.4372 m, and 0.496 m, respectively. A safety margin of ±10 cm was applied to all calculated levels as per the Naval Recruiting and Training Agency (NRTA). Statistical analysis of the observed sea level data revealed a range of 1.81 m, with the highest observed water level at 19.128 m and the lowest at 17.318 m, with a standard deviation of 0.16 m, all referenced to the ESA zero level. The study also found a consistent 20 cm difference in LAT between 1906 and 2015, attributed to the IHO's 2011 redefinition of LAT. It is recommended that the HAT and LAT values be updated in all relevant nautical publications to 18.72 m and 18.01 m, respectively, resulting in an astronomical tidal level range of 0.516 m relative to the ESA zero datum.

Table 2: Concise summary of tidal levels for the Port Said Shoreline.

Tidal Parameter	Value (m)
Mean High Water Springs (MHWS)	18.33
Mean Low Water Springs (MLWS)	17.96
Mean High Water Neaps (MHWN)	18.14
Mean Low Water Neaps (MLWN)	18.05
Highest High Water Level (HHWL)	19.128
Lowest Low Water Level (LLWL)	17.318
Highest Astronomical Tide (HAT)	18.72
Lowest Astronomical Tide (LAT)	18.01

Source: Authors.

3.2. Model.

3.2.1. Model Description.

The LITPACK system is a coastal modeling system developed by DHI (Water & Environment). This software aims to aid in simulating critical functions of the nearshore regions. It combines several particular modules that deal with modeling river and ocean coastal sediment transport as well as shoreline development. Thus, it forms a solid basis for solving complicated coastal engineering problems. It does allow a high degree of accuracy. As an example, in the case of the engagement of several quite complex factors (cross waves, varying grain size and bed slope, etc.) a more accurate prediction will be obtained than solutions of semi-empirical rules(Mansour et al., 2024).

LITPACK contains multiple modules that are interrelated but focus on different aspects of the coastal processes. First, the STP (Sediment Transport Module) forms the basis of all calculations regarding sediment movement including sand, where sand transport is calculated due to the influence of the waves and currents. The modeling of longshore currents and littoral drift currents is done in the LITDRIFT module. The LITLINE on the other hand uses a one-line model of the shoreline evolution which entails the one-dimensional solution of the sediment continuity equation in the littoral zone. Furthermore, LITTREN deals with sedimentation in trenches, and LITPROF looks into the forcing of reproduction of cross-shore profiles regarding sediment transport to the beaches and profiles. The automation is responsible for controlling the settings of the integration of these modules (Mohamed et al., 2023).

The selection of LITPACK for this study was based on its deterministic framework that captures the complex interface between hydrodynamic forces and sediment movement. Unlike semi-empirical models, LITPACK incorporates the most critical issues such as multi-barred beach profiles, sediment grain distributions, and bed slope effects. Such capacity becomes critical in the area of sediment transport and shoreline evolution in the area due to the existence of such complexity (DHI Water and Environment, 2023).

Some factors have been identified to affect the performance of the model. Achieving reliable simulations requires wave climate to be captured accurately in the form of wave height, period, and direction. The composition of sediments, especially the median size and the distribution of bed materials greatly affect the rate of sediment transport. Moreover, the use of a high-resolution dataset on the coastal bathymetry permits an accurate representation of the spatial distribution of the nearshore zone which is critical in the modeling of sediment transport and coastline transformations due to natural and anthropogenic factors (Larson et al., 2007).

LITLINE calculates shoreline changes by solving a continuity equation for sediment within the littoral zone (Subiyanto and Supian, 2021). The continuity equation for sediment volumes is:

$$\frac{dy_c}{dt} = -\frac{1}{h_{act}}\frac{dQ}{dx} + \frac{Q_{sou}}{h_{acr}\,\Delta x} \tag{1}$$

Where:

y_c : is the Position of the coastline (distance from the baseline to the shoreline),

t : is the time,

x : is the long-shore position,

$Q_{(x)}$: is the long-shore transport rate along the coast, expressed in a volume,

$Q_{sou(x)}$: is source/sink term, expressed in volume/Δx, and

h_{act} : The height of the active cross-shore profile is determined by three components: the active depth relative to the mean water level (DC), the height of the beach above the mean water level that moves with the coastline position (DB), and the presence of dunes, which may erode during erosive events but do not recover during accretion phases.

The evolution in time is determined by solving equation 1, using an implicit Crank-Nicholson scheme(Tolba, 2012).

LITDRIFT involves calculating both the long-shore current and sediment transport (Mangor et al., 2017).

The Total Sediment Transport (q_t)is split into bed load (q_b) and suspended load (q_1), which is calculated separately. The transport of non-cohesive material as bed load is calculated according to the model presented by (Engelund and Fredsoe, 1976). The bed load transport (q_b) is determined as a function of the bed shear stress through the dimensionless bed shear stress (ϑ)

$$\vartheta = \frac{{U_f}^2}{(S-1)\;g\,\sigma} \tag{2}$$

Where:

ϑ : is the bed load transport,

U_f : is the shear velocity,

S : is the relative sediment density,

g : is the acceleration of gravity,

σ : is the fall diameter of sediment particles.

The suspended sediment transport (q_1), is calculated as the product of sediment concentration and the mean circulation current averaged over the wave period (T) (Flensberg et al., 1988).

$$q_1 = \frac{1}{T}\int_0^T \int_{2\sigma}^D C\, U_{mean}\, d_y\, d_t \tag{3}$$

Where:

q_1 : is the suspended sediment transport,
T : is the wave period,
σ : is the fall diameter of sediment particles,
D : is the grain size,
C : is the sediment concentration,
U_{mean} : is the summation of the Eulerian circulation current and the Lagrangian drift velocity obtained from the flow model.

3.2.2. Model Setup and Simulation Process.

This study investigates shoreline evolution near the El - Manzala Lake Main Tidal Inlets Jetties on Egypt's northeastern coast, employing the 1-D LITPACK model to assess the impact of jetty extensions on the stability of Port Said's shoreline. The analysis focuses on a 7.5 km coastal stretch, spanning approximately 3 km eastward and 4.5 km westward from the main tidal inlets, encompassing the western jetties of the second lake as seen in Fig. 7. Shoreline changes between 2019 and 2022 are simulated using the DHI-LITLINE module, while alongshore sediment transport is computed via the DHI-LITDRIFT surf zone model. Five shore-normal cross-shore profiles are defined to capture bathymetric variability and sediment transport dynamics. These profiles are positioned at 1,000 m, 2,000 m, 3,000 m, 5,000 m, and 7,000 m alongshore distances from the reference line (aligned with the main tidal inlet). The distance between consecutive profiles varies, with intervals of 1.0 km between the first three profiles and 2.0 km between the latter two, reflecting the focus on critical zones near the inlets, ensuring coverage of critical hydrodynamic zones. Each profile is oriented perpendicular to the baseline datum (shore-normal) and aligned with the groins and jetties, ensuring consistency with coastal structures. Cross-shore bathymetric data for these profiles include depth measurements at incremental distances from the shoreline, capturing nearshore slopes and seabed morphology. The eastern profiles (1.0–3.0 km) traverse areas of active sediment dynamics due to jetty influences, while the western profiles (5.0–7.0 km) reflect transitional zones where longshore currents diminish.

Wave, wind, and tide data are incorporated as inputs to the one-line model. Wave climate is represented by directional bins (significant wave height, period, and direction) with corresponding frequency of occurrence, derived from historical records and regional hindcast databases. Tide levels and currents are prescribed as time-series data, while wind inputs include speed and direction to account for aeolian sediment transport effects. Sediment properties (median grain size: 0.2–0.3 mm) and the initial 2019 shoreline configuration (digitized from Mirdan et al., 2023) are integrated to establish baseline conditions. Structural elements, such as groins and jetties, are modeled as impermeable barriers aligned parallel to longitude lines and perpendicular to the baseline.

The model employs a variable spatial resolution alongshore, with profile spacing tailored to resolve key morphodynamic features. Cross-shore resolution is defined by the five profiles, while the alongshore grid is discretized at 50–100 m intervals to balance computational efficiency and accuracy. Temporal resolution is set to monthly time steps over the 2019–2022 simulation period, capturing seasonal variability in wave climate and sediment transport.

The LITDRIFT and LITLINE modules are calibrated using field-measured sediment transport rates and historical shoreline positions (Ari Guner and Yumuk, 2014). Wave forcing and bathymetric parameters are iteratively adjusted to minimize discrepancies between modeled and observed data. Validation is performed using Landsat imagery (30 m resolution), with shoreline positions extracted at six-month intervals. Fig. 8 outlines the phases of the simulation process, employing the LITLINE and LITDRIFT modules to compute the results.

Figure 7: LITPACK 1D model setup.

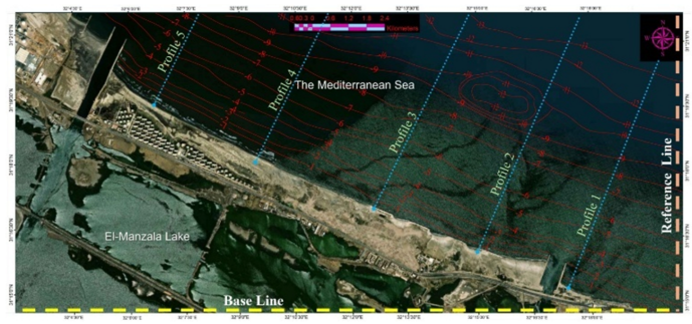

Source: Authors.

Figure 8: Processing flowchart of the simulation.

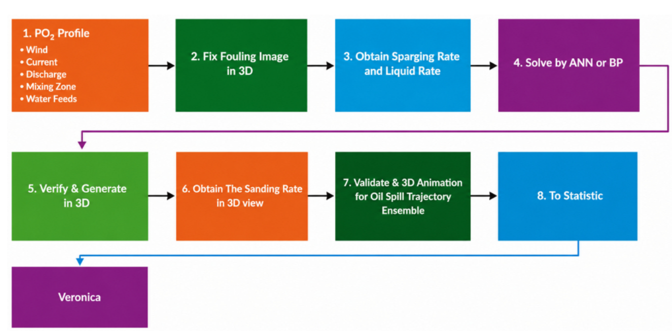

Source: Authors.

4. Results.

4.1. Calibration and Validation.

The simulation of shoreline alterations from 2019 to 2022 within the geographic scope of the study involved a meticulous calibration and validation process. Calibration was initiated by utilizing the measured shoreline data from 2019 as a reference to simulate the shoreline conditions of 2020. Subsequently, the simulated 2020 shoreline was compared with the measured

2020 shoreline to fine-tune the model parameters. The calibration process primarily relies on two sensitive parameters: the extension of the sediment transport table and the active depth (Saha et al., 2017). The extension of the sediment transport table, defined as the distance from the actual shoreline to the surf zone, was varied with values of 0.0, 70, 100, and 120 meters, as shown in Fig. 9a. The active depth, revised to reflect the sum of the berm height (2 m, based on field surveys) and the depth of closure (10 m, calculated using Hallermeier, 1981 formula).

Hallermeier's closure depth (h_c) was computed as:

$$h_c = 2.28H_s - \frac{68.5H_s^2}{g\,T^2} \tag{4}$$

Where:

H_s : is the mean significant wave height and equal 3.20 meter,

T: is the mean wave period derived from 2019–2020 wave data and equal 8 seconds.

yielding h_c=10 m. The total active depth (h_a) is thus h_a= h_c+ berm height =12 m.

A wave diffraction spreading factor of 25 was also selected to determine the wave concentration parameter in deep water.

Further adjustments to the active depth or expansion of sediment transport tables were contemplated for the final calibration to align the predicted shoreline evolution with observed changes. The root mean square percentage error (RMSPE) is used to quantify the errors in the simulation results. The corresponding equation was previously provided by (Liu et al., 2011):

$$RMSPE = \sqrt{\frac{1}{N}\sum_{i=1}^{N}\left\{100\frac{(Y_s)_i - (Y_0)_i}{(Y_0)_i}\right\}^2} \tag{5}$$

Where:

$RMSPE$: is the root mean square percentage error,

$(Y_s)_i$: is the distance from the baseline to the simulated shoreline,

$(Y_0)_i$: is denotes the distance from the baseline to the observed shoreline, and

N: is the number of segments.

Boundary conditions were carefully defined to minimize artifacts. Pinned boundaries were placed 2 km beyond the study area's eastern/western limits to avoid influencing the inlet dynamics. The groins northwest of tidal inlet B were explicitly incorporated into the model domain, with their impact on southeast-directed sediment transport represented through reduced longshore transport coefficients in their vicinity.

Fig. 9b presents the RMSPE results and their corresponding extended transport table parameters. The lowest RMSPE, calculated at 2.18%, corresponds to a 70 m extension of the sediment transport table. Therefore, this 70 m value is suitable as a tuning parameter for quantifying shoreline changes. Fig. 9c shows the calibration results using the observed 2020 shoreline at the same 70 m extension. The model effectively predicts severe accretion rates ranging from +15 m/year to +24 m/year to the west of the inlet and accurately predicts erosion rates ranging from -7 m/year to -16 m/year to the east of the inlet, which are closely comparable to the rates determined from measured data by (Mirdan et al., 2023).

Figure 9: Calibration process. (a) The shoreline measured in 2019 with different extensions of the transport parameter; (b) the shoreline residuals and their corresponding RMSPE values; and (c) the 1-year simulated shoreline changes.

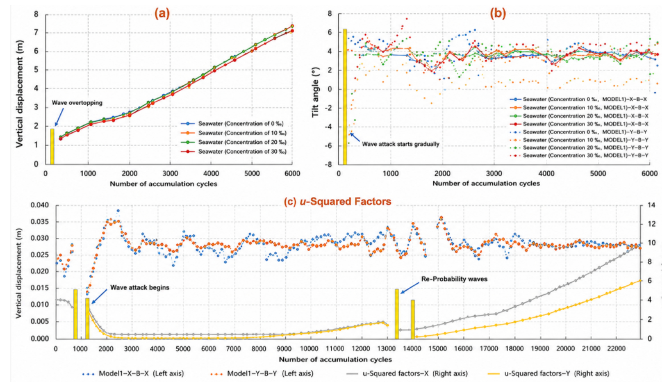

Source: Authors.

Following calibration, the model's validation employed the predicted 2020 shoreline, derived from the model, as a reference to simulate the shoreline in 2022. The measured 2022 shoreline, digitized from satellite imagery by (Mirdan et al., 2023), was then compared with the predicted one to assess the model's accuracy and validate its predictive capabilities, as we can see in Fig. 10. The model exhibited notable accuracy in predicting the erosion rate along the eastern section of the main tidal inlet jetties, ranging from 5 to 10 meters per year, while successfully anticipating accretion rates between 8 to 18 meters per year in the western segment. The model's performance was robust with a standard deviation error of 3.72 meters, within acceptable limits for a 1D model, especially considering the expansive 8-kilometer shoreline.

Figure 10: Validation process.

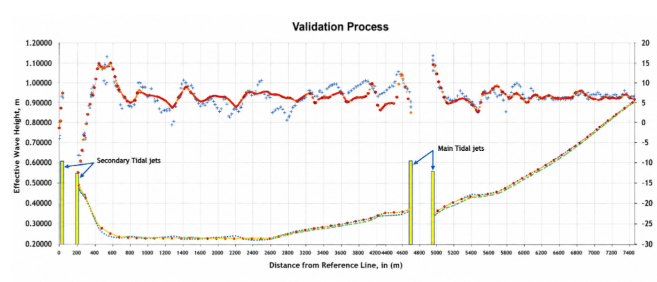

Source: Authors.

Comparative analysis against observed data post-calibration validated its fidelity in replicating current shoreline-changing dynamics in the research area. Beyond calibration, the model's versatility was demonstrated in forecasting the effects of different scenarios on water levels and coastal drift, considering hourly incident waves from 2020 to 2040. Furthermore, it accurately simulated the existing coastal state, including its current structures.

In practice, LITPACK offers limited boundary condition options, primarily allowing pinned boundaries. A pinned boundary condition implies that the boundary remains fixed at the initial shoreline position throughout the calculation period. To minimize boundary effects, it is generally recommended to position pinned boundaries far from the area of interest. The study has now clarified that the presence and influence of groynes northwest of tidal inlet B were taken into account, as they significantly impact longshore sediment transport directed towards the southeast.

Finally, since the role of structures such as jetties in influencing sediment transport is central to this study, it is essential to explicitly illustrate how sediment transport patterns vary across different scenarios. Instead of focusing solely on shoreline position changes, incorporating visualizations or quantitative assessments of sediment flux variations would enhance the robustness of the analysis and further validate the model's applicability to coastal engineering applications.

This comprehensive revision ensures that calibration procedures are transparent, boundary conditions are well-defined, and sediment transport dynamics are appropriately contextualized, thereby improving the study's overall rigor and scientific contribution.

4.2. Model Application under Different Scenarios.

Following rigorous calibration and validation procedures, the numerical model was employed to project the potential impacts of diverse scenarios between shoreline conditions in 2020 and projected scenarios for 2040. This encompassed forecasting the effects of plausible changes on the shoreline's dynamics. Moreover, the model was utilized to simulate the repercussions on the shoreline's evolution while incorporating the existing structures and coastal elements. This comprehensive approach aimed to provide insights into the potential trajectory of shoreline alterations and their implications over the two-decade period. It offers a valuable understanding of the region's coastal dynamics and contributes to informed decision-making in coastal management and planning.

4.2.1. Scenario (0): Benchmark (the current status of the shoreline with the established structures).

The model's simulation, covering a distance of 7500 meters near EL-Manzala Lake's main tidal inlet jetties, focused with precision on a 5500-meter stretch adjacent to the main tidal inlets to forecast shoreline changes from 2020 to 2040. The base case was established as a benchmark, representing the current scenario devoid of additional protective structures. Through the LITE LINE model, projections unveiled a conspicuous erosion pattern along the eastern side of the main tidal inlet jetty, revealing a maximum erosion of -112.50 meters by 2040. In stark contrast, a notable deposition of approximately +138 meters emerged along the western side of the main tidal inlet jetty, as seen in Fig. 11. The western jetty's interruption of long-shore sediment transport led to sediment accumulation on its western side, while the along-shore current's impact on the inlet's downdrift side precipitated significant shoreline erosion and retreat on the eastern front.

Figure 11: The shoreline forecast for 2040's Scenario 0 (i.e., benchmarks).

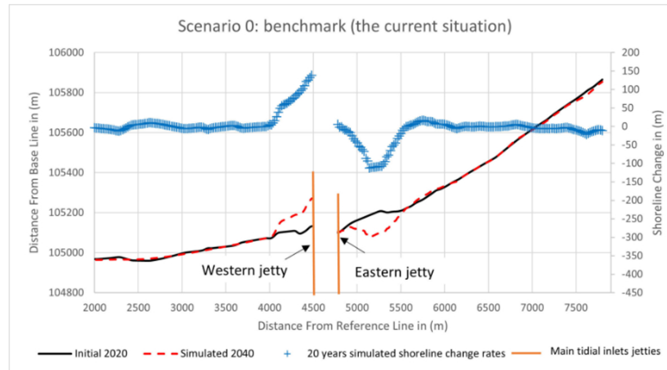

Source: Authors.

4.2.2. Scenario 1: Establish four groins east of the inlet.

Proposed defense structures for mitigating erosion within the critical area (4800 to 7200 meters eastward) were outlined, focusing on the establishment of four groins along the eastern side of the main tidal inlet jetty. These suggested groins, each 250 meters in length with a 400-meter spacing between them (positioned at distances 5500 to 7200 meters, equivalent to 1100 to 2800 meters from the Reference line as seen in Fig. 12, were evaluated against the benchmark scenario depicting the current shoreline condition with existing structures. A comparison of results between the proposed scenario with the groins and the benchmark scenario revealed promising trends. The construction of these groins demonstrated a substantial reduction in erosion rates, notably decreasing from -112.5 meters in the benchmark scenario to -17 meters over a twenty-year period.

Figure 12: Shoreline Projection Scenario 1 for 2040.

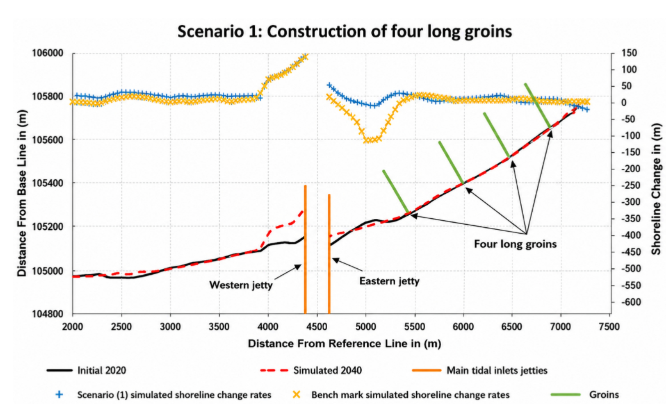

Source: Authors.

However, some areas between the groins experienced heightened erosion, with instances of increased erosion reaching 20 meters after the construction of the first groin, compared to a maximum erosion of -2 meters in the same section without groin construction over the same duration. Overall, while this scenario marginally alleviated erosion along the eastern side of the main tidal inlets, it also led to increased erosion in select areas between the constructed groins.

4.2.3. Scenario 2: Establish five detached Breakwaters east of the inlet.

Simulating the establishment of five detached breakwaters along the eastern side of the main tidal inlet jetty, positioned within distances ranging from 5000 to 6800 meters (equivalent to 900 to 2700 meters from the reference line), constituted a significant aspect of this scenario. Each suggested breakwater, 200 meters in length with 200-meter spacing in between, was strategically placed approximately 180 meters offshore from the main tidal inlet jetty, oriented at right angles to the prevailing wave direction, and designed with an active depth of five meters, as seen in Fig. 13. Evaluation of this scenario against the benchmark scenario reflecting the current shoreline condition with established structures revealed notable outcomes. The construction of these breakwaters instigated the formation of salient, influenced by circulation currents resulting from wave run-up and run-down, as well as wave crest interactions behind the breakwaters. Consequently, compared to the benchmark, these salient significantly altered the erosion pattern, mitigating erosion by approximately 40.65%. However, the transmission of wave energy through the gaps between breakwaters sustained shoreline retreat at a maximum rate of +20 meters over 20 years within these sections. In summary, this scenario exhibited promising outcomes over a 20-year period when contrasted with the benchmark scenario, showcasing substantial improvements in erosion mitigation and shoreline stability.

Figure 13: Shoreline Projection Scenario 2 for 2040.

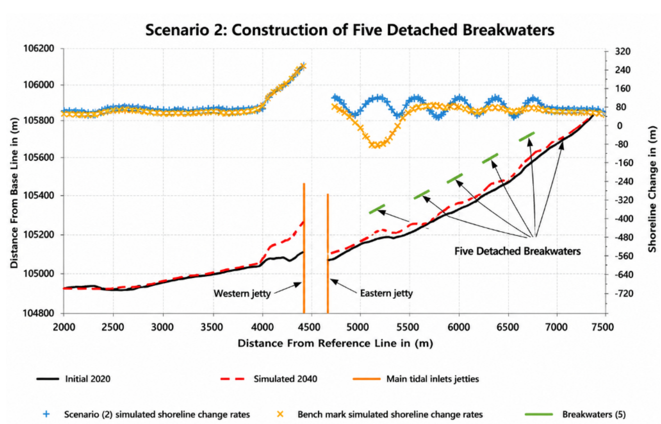

Source: Authors.

4.2.4. Scenario 3: Establish five submerged detached Breakwaters east of the inlet.

Modeling the implementation of five submerged detached breakwaters along the eastern side of the main tidal inlet jetty, positioned within distances spanning 5000 to 6800 meters (equivalent to 900 to 2700 meters from the reference line), formed a pivotal aspect of this scenario. These suggested breakwaters, each 200 meters in length with 200-meter spacing between them, were strategically placed approximately 180 meters offshore from the main tidal inlet jetty, oriented perpendicular to the prevailing wave direction, and designed with an active depth of two meters, as seen in Fig. 14. Evaluation against the benchmark scenario representing the current shoreline condition with established structures revealed significant findings. The construction of these submerged breakwaters resulted in the formation of salient, although to a lesser extent compared to emerged breakwaters. Despite this, the salient notably influenced the erosion pattern, effectively reducing erosion by approximately 30.78% when compared to the benchmark scenario. This scenario showcases the promising potential of submerged detached breakwaters in mitigating erosion and shaping shoreline stability, offering valuable insights into their efficacy over the assessed timeframe.

Figure 14: Shoreline Projection Scenario 3 for 2040.

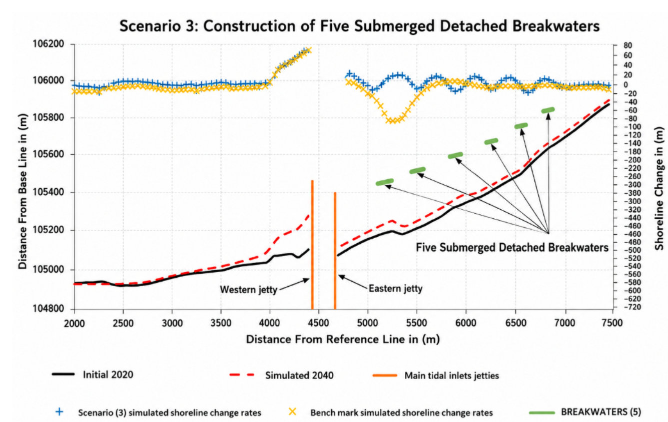

Source: Authors.

4.2.5. Scenario 4: usage of 150,000 cubic meters of sand nourishment per year.

In this scenario, a deliberate intervention was made by introducing 150,000 cubic meters per year of sand nourishment along the east main tidal inlet jetty, spanning a distance of 1600 meters from 4800 to 6400 meters (equivalent to 1100 to 2700 meters measured from the model's reference line), as seen in Fig. 15. This deliberate sand nourishment, when compared to the benchmark scenario, demonstrated significant efficacy in mitigating coastline erosion along the eastern side of the inlet. Over 20 years, the nourished area exhibited a transformation from erosion measuring -110 meters to approximately -10 meters. The results vividly showcase the complete mitigation of erosion within the nourished area. The nourished sand effectively counteracted erosion, underscoring its potential as an impactful strategy for shoreline stabilization and erosion prevention over the assessed duration.

Figure 15: Shoreline Projection Scenario 4 for 2040.

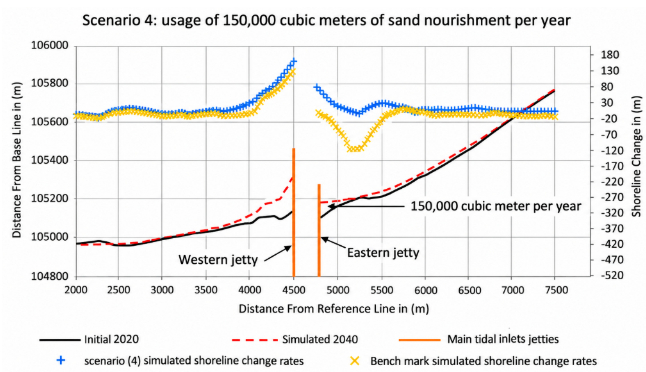

Source: Authors.

4.2.6. Scenario 5: Establish four groins and four detached Breakwaters east of the inlet.

Proposing a combined approach of groins and detached breakwaters along the eastern edge of the major tidal intake presents a robust strategy for shoreline protection. The simulation includes the construction of four detached breakwaters positioned between distances of 5000 to 7000 meters (equivalent to 1200 to 2700 meters from the reference line) and groins established at the same positions as scenario 1, each groin with a length of 250 meters and a spacing of 400 meters within distances of 5500 to 7200 meters (1100 to 2800 meters from the reference line). Situated approximately 180 meters from the shoreline and oriented at right angles to the prevailing wave direction, these breakwaters, each 250 meters long and wide with an active water depth exceeding 5.0 meters, as seen in Fig. 16.

Figure 16: Shoreline Projection Scenario 5 for 2040.

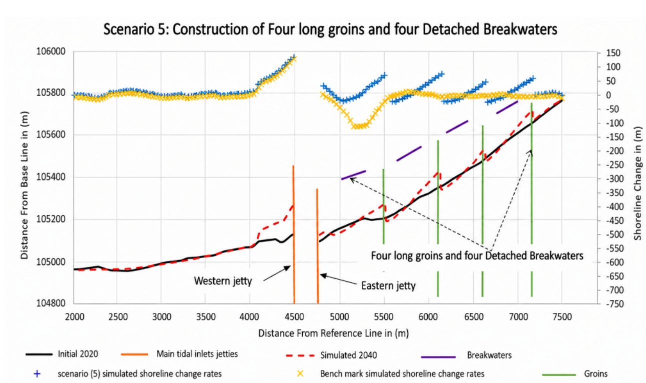

Source: Authors.

Comparing the simulation results with the benchmark scenario revealed a remarkable reduction in predicted erosion when employing a combination of detached breakwaters and groins, outperforming scenarios employing either groin alone or detached breakwaters solely. The interplay between groins and breakwaters fostered the creation of an energetic salient, driven by circulation currents transporting eroded silt to sheltered areas behind the breakwaters. This dynamic differed when employing breakwaters alone, resulting in a 1.79% reduction in erosion. The presence of lengthy groins notably curtailed eastward littoral drifts, inducing significant accumulation on the updrift side and a maximum shoreline recession of -18 meters over 20 years on the downdrift side.

4.2.7. Scenario 6 Establish three groins and three detached Breakwaters (three T groins) east of the inlet.

Proposing a system of three T groins" a composite arrangement of detached breakwaters and groins" along the eastern side of the main tidal inlet jetty represents a robust strategy for shoreline protection. The suggested groins, each 400 meters in length with a spacing of 700 meters between them within distances of 5500 to 7200 meters (equivalent to 1100 to 2800 meters from the reference line), coupled with three detached breakwaters established perpendicular to the groins at distances spanning 5000 to 7000 meters (1200 to 2700 meters from the reference line). These breakwaters, 250 meters in length with 500 meters spacing in between, were placed 180 meters offshore from the main tidal inlets' jetty with an active depth of five meters, as seen in Fig. 17. The simulation results, compared against the benchmark scenario, demonstrated a significant reduction in predicted erosion when employing detached breakwaters in conjunction with extended groins, surpassing scenarios utilizing either groins alone or detached breakwaters solely. With an average erosion of -8 meters over 20 years within the system, this configuration notably impacted the lower drift side, showcasing an effective and discernible alteration in erosion patterns.

Figure 17: Shoreline Projection Scenario 6 for 2040.

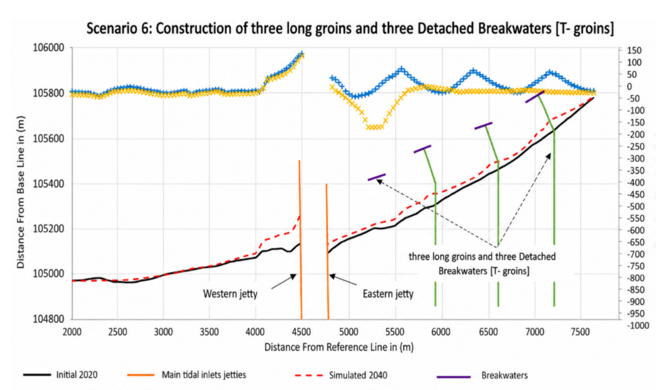

Source: Authors.

4.2.8. Scenario 7 Establish a rubble mound seawall east of the inlet.

The proposition of a rubble mound seawall along the eastern side of the main tidal inlet jetty emerged as a viable strategy for shoreline stabilization. This suggested seawall, extending 500 meters within distances of 4800 to 5200 meters (equivalent to 3000 to 3500 meters from the Reference line), exhibited significant efficacy in curbing coastal erosion. Upon comparison with the benchmark scenario, the simulation results revealed a remarkable reduction in erosion along the eastern side of the inlet. Over 20 years, the installation of the rubble mound seawall resulted in transformative shoreline stability, mitigating erosion from -110 meters to nearly -5 meters. Notably, the shoreline remained balanced and stable, indicating the compelling effectiveness of the seawall in curbing erosion and fostering shoreline equilibrium over the simulated timeframe, as seen in Fig. 18.

Figure 18: Shoreline Projection Scenario 7 for 2040.

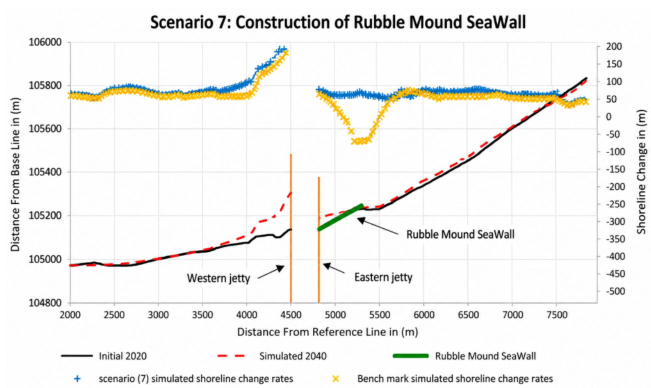

Source: Authors.

4.2.9. *Scenario 8: annual dredging of 100,000 cubic meters at a distance of 450 m left the western Jetty of the inlet.*

While the installation of protective jetties presents a promising short-term solution to mitigate sand sedimentation within the El-Manzala Lagoon inlets, the persisting issue of sedimentation necessitates additional strategies. In this scenario, the simulation involves an annual dredging operation of 100,000 cubic meters, strategically implemented along a 450 - meter stretch to the left of the western jetty of the main tidal inlets, covering distances of 4050 to 4500 meters (equivalent to 3000 to 3450 meters from the reference line).

Figure 19: Shoreline Projection Scenario 8 for 2040.

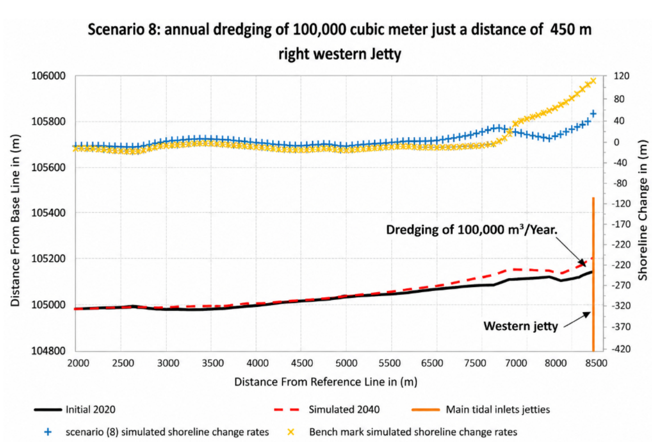

Source: Authors.

Simulation results demonstrate the superior efficacy of this approach in optimizing sedimentary stock to the west of the inlet. Over 20 years, the scenario effectively mitigates sedimentation, reducing sedimentary stock from +138.50 meters in the benchmark scenario to +68.50 meters. This strategy showcases promise in managing sedimentation and maintaining a more balanced sedimentary equilibrium within the studied area, as seen in Fig. 19.

5. Discussion.

5.1. *Analysis of the Results.*

The study utilized a 1D-LITPACK numerical model to assess the impact of extending inlet jetties along a 7.50 km shoreline stretch. The focus was on understanding how these extensions affect erosion and accretion rates around the jetties over 20 years starting from 2020. The findings highlighted an average shoreline erosion of -110 meters on the down-drift side of the main tidal inlet jetties. To address this, the study proposed eight scenarios aimed at mitigating erosion. The first scenario involved constructing four long groins east of the inlet, which reduced average erosion rates to -16.75 meters over 20 years. The second and third scenarios proposed the construction of five detached breakwaters (emerged or submerged) east of the inlet. The emerged breakwaters demonstrated substantial improvements, achieving zero erosion and a shoreline advancement of +35 meters over 20 years compared to the submerged breakwaters. Another scenario suggested the annual usage of 150,000 cubic meters of sand nourishment in the east main tidal inlet jetty area. This approach effectively alleviated shoreline erosion, maintaining a balanced nourished area. The fifth scenario combined detached breakwaters with long groins, significantly reducing predicted erosion. The sixth scenario involved establishing three groins and three detached breakwaters (three T groins) east of the inlet, demonstrating considerable erosion reduction compared to using groins or detached breakwaters alone. The seventh scenario, involving a rubble mound seawall east of the inlet, emerged as the most effective solution, stabilizing the shoreline over the 20-year simulation period. Lastly, the simulation of annual dredging of 100,000 cubic meters on the up-drift side of tidal inlet jetties showed superior results in optimizing sedimentary stock to the west of the inlet, reducing it from 138.50 meters to 68.50 meters over 20 years. Overall, the study explored multiple scenarios and their impact on mitigating erosion around inlet jetties, with findings indicating that strategies like emerged breakwaters, sand nourishment, combined groins and breakwaters, and a rubble mound seawall show promise in stabilizing and reducing erosion along the shoreline.

5.2. *Choosing the Best Scenario among the Simulated Scenarios.*

Choosing the optimal scenario involves considering various factors such as project objectives, budget limitations, environmental impacts, and site-specific characteristics. Each scenario has its own set of benefits and drawbacks. Based on the provided information, here are some key considerations for selecting the best scenario: Scenario 4 (Sand Nourishment) and Scenario 7 (Rubble Mound Seawall) show significant hydraulic effectiveness by greatly reducing erosion and stabilizing the shoreline. In terms of cost considerations, Scenario 4

(Sand Nourishment) and Scenario 8 (Annual Dredging) require less intensive construction, potentially resulting in lower initial costs compared to more substantial infrastructure projects like breakwaters or seawalls. From a sustainability and environmental impact perspective, Scenario 4 (Sand Nourishment) is a more sustainable option compared to hard engineering structures like seawalls or breakwaters, as it utilizes natural processes and materials. Additionally, Scenario 4 (Sand Nourishment) may have reduced long-term maintenance needs compared to structures like seawalls or breakwaters. When evaluating site-specific considerations, it is important to assess the specific conditions of the EL-Manzala Lake area, including wave patterns, sediment transport, and ecological sensitivity. Some scenarios may be more appropriate based on these site-specific factors. Regulatory compliance is another crucial factor; consider the ease of obtaining regulatory approvals for the chosen scenario, as some projects may encounter more challenges in terms of environmental impact assessments and permitting. Given these factors, Scenario 4 (Sand Nourishment) seems to be a strong candidate. It offers effective erosion control, is potentially more cost-effective, and has a lower environmental impact compared to some engineering structures. However, it is essential to consult with local experts, environmental agencies, and stakeholders to ensure the selected scenario meets the specific needs and conditions of the EL-Manzala Lake area.

Conclusions.

This study provides an in-depth analysis of the impacts of recent jetty extensions at the main tidal inlets of El-Manzala Lake on sediment transport and shoreline stability along the coastal stretch between Damietta and Port Said. Various scenarios were simulated using the LITPACK numerical model to understand the hydrodynamic and sedimentary responses to these modifications over a 20-year period.

The findings reveal that jetty extensions have significantly influenced sediment dynamics, causing notable erosion on the downdrift side and accretion on the updrift side of the inlets. Among the eight scenarios evaluated, the construction of emerged breakwaters and the implementation of sand nourishment were identified as the most effective strategies for mitigating erosion and stabilizing the shoreline. Specifically, sand nourishment demonstrated a balanced approach by leveraging natural processes to counteract erosion with minimal environmental impact.

The results underscore the importance of tailoring coastal management strategies to site-specific conditions. Protective structures, such as groins and breakwaters, effectively altered sediment transport patterns; however, these interventions must be carefully planned to avoid unintended negative consequences, such as exacerbating erosion in adjacent areas. Combining hard engineering solutions with soft measures like sand nourishment showed promise for achieving sustainable outcomes.

The study highlights the dynamic nature of coastal systems, emphasizing the necessity for ongoing monitoring and adaptive management to address changes in sediment dynamics and shoreline morphology. While the modeling results provide a basis for understanding the impacts of the jetty extensions, further studies focusing on long-term changes and external factors such as climate variability and sea-level rise would complement this analysis.

In conclusion, this research contributes valuable insights into the sedimentary and hydrodynamic responses to infrastructure modifications along the Egyptian Mediterranean coast. The findings provide a scientific foundation for developing strategies that prioritize both coastal protection and the preservation of natural processes, supporting the sustainable management of these vital regions.

Conflict of Interest.

We wish to confirm that there are no known conflicts of interest associated with this publication and there has been no significant financial support for this work that could have influenced its outcome.

Funding sources.

This research did not receive any specific grant from funding agencies in the public, commercial, or not-for-profit sectors.

Data Availability.

Some or all data, models, or code that support the findings of this study are available from the corresponding author upon reasonable request.

Acknowledgments.

The authors will later thank the editors and reviewers for their efforts.

References.

Abd Abd Ellah, R.G., 2022. Using single-beam bathymetric data technique to estimate dredging: a case study in Lake Manzala (Egypt). Arabian Journal of Geosciences 15. https://doi.org/10.1007/s12517-022-10937-2.

Abdelaal, A., Abdelkader, A., Alshehri, F., Elatiar, A., Almadani, S., 2022. Assessment and Spatiotemporal Variability of Heavy Metals Pollution in Water and Sediments of a Coastal Landscape at the Nile Delta. Water (Basel) 14, 3981. https://doi.org/10.3390/w14233981.

Abd-Ellatif, M., Guerretti, V., Rashad, H., Zaghloul, M., Moustafa, A., 2024. Impact of a dredging project on waterbird diversity and water and sediment quality in Ashtoum El-Gamil protected area, Egypt: a first seasonal overview. EuroMediterr J Environ Integr 12. https://doi.org/10.1007/s41207-024-00490-7.

Ali, E.M., El-Magd, I.A., 2016. Impact of human interventions and coastal processes along the Nile Delta coast, Egypt during the past twenty-five years. Egypt J Aquat Res 42, 1–10. https://doi.org/10.1016/j.ejar.2016.01.002.

Ali W, K., MF, K.S., M., E.-T., 2017. Assessment of shoreline stability and solidity for future investment plans at Ras El-Bar Resort (EGYPT). www.ejabf.js.iknito.com Egyptian Journal of Aquatic Biology & Fisheries 21. https://doi.org/10.1016/-j.agrformet.2007.11.012.

Anton, I.A., Panaitescu, M., Panaitescu, F. V., 2017. Optimizing romanian maritime coastline using mathematical model Litpack. IOP Conf Ser Mater Sci Eng 227. https://doi.org/10.1-088/1757-899X/227/1/012009.

Ari Guner, H., Yumuk, H., 2014. Application of a fuzzy inference system for the prediction of longshore sediment transport. Applied Ocean Research 48, 162–175. https://doi.org/10-.1016/j.apor.2014.08.008.

Beck, T.M., Wang, P., Li, H., Wu, W., 2020. Sediment Bypassing Pathways between Tidal Inlets and Adjacent Beaches. J Coast Res 36, 897–914. https://doi.org/10.2112/JCOASTRES-D-19-00141.1.

Bruun, P., 1966. Tidal Inlets and Littoral Drift. Journal of Waterways and Harbors Division, ASCE.

Chan, M., 2024. A criterion for sustainably stable tidal inlets. Coastal Engineering 188, 104445. https://doi.org/10.1016/-j.coastaleng.2023.104445.

Dewidar, K.M., Frihy, O.E., 2003. Thematic Mapper analysis to identify geomorphologic and sediment texture of El Tineh plain, north-western coast of Sinai, Egypt. Int J Remote Sens 24, 2377–2385. https://doi.org/10.1080/01431160110115807.

DHI Water and Environment, 2023. Software catalogue 2023.

El Banna, M.M., Hereher, M.E., 2009. Detecting temporal shoreline changes and erosion/accretion rates, using remote sensing, and their associated sediment characteristics along the coast of North Sinai, Egypt. Environmental Geology 58, 1419–1427. https://doi.org/10.1007/s00254-008-1644-y.

El-Asmar, H., Taha, M., 2022. Monitoring Coastal Changes and Assessing Protection Structures at the Damietta Promontory, Nile Delta, Egypt, to Secure Sustainability in the Context of Climate Changes. Sustainability 14, 15415. https://doi.org/-10.3390/su142215415.

ElKotby, M.R., Sarhan, T.A., El-Gamal, M., 2023. Assessment of human interventions presence and their impact on shoreline changes along Nile delta, Egypt. Oceanologia 65, 595–611. https://doi.org/10.1016/j.oceano.2023.06.008.

Elshemy, M., 2017. Environmental and Climatic Implications of Lake Manzala, Egypt: Modeling and Assessment, in: Handbook of Environmental Chemistry. https://doi.org/10.100-7/698_2017_109.

Eltokhi, M., 2008. Impact of Heavy metals and Petroleum Hydrocarbon of the East Port Said Port area, Egypt. J Appl Sci Res 412: 178, 1788–1798.

Engelund, F., Fredsoe, J., 1976. A Sediment Transport Model for Straight Alluvial Channels, NORDIC HYDROLOGY.

Escoffier, F.F., 1940. The Stability of Tidal Inlets. Shore and Beach, ASBPA.

FitzGerald, D., Miner, M., 2021. Tidal Inlets and Lagoons Along Siliciclastic Barrier Coasts, in: Reference Module in Earth Systems and Environmental Sciences. https://doi.org/10-.1016/B978-0-12-818234-5.00079-1.

Flensberg, K., Hedeg\aard, P., Brix, M., 1988. Asymmetry in the normal-metal to high-${T}_{c}$ superconductor tunnel junction. Phys. Rev. B 38, 841–843. https://doi.org/10.1103-/PhysRevB.38.841.

Gong, J., Burningham, H., 2024. Multivariate analysis of inlet morphodynamics: The mixed sand-gravel ebb-tidal delta of Deben Estuary, Suffolk. Geomorphology 454, 109163. https:-//doi.org/10.1016/j.geomorph.2024.109163.

Halawany, E.-, Transport, M., Academy, A., Transport, M., 2022. Tidal Datum Levels Realization based on observed Sea level data analysis in Port Said, Egypt. AIN Journal 44, 31–38.

Hallermeier, R.J., 1981. Terminal settling velocity of commonly occurring sand grains. Sedimentology 28, 859–865. https://doi.org/10.1111/j.1365-3091.1981.tb01948.x.

Hanegan, K.C., FitzGerald, D.M., Georgiou, I.Y., Hughes, Z.J., 2023. Long-term sea level rise modeling of a basin-tidal inlet system reveals sediment sinks. Nat Commun 14, 7117. https://doi.org/10.1038/s41467-023-42895-y.

Holthuijsen, L.H., 2007. Waves in Oceanic and Coastal Waters. Cambridge University Press, Cambridge. https://doi.org/-DOI: 10.1017/CBO9780511618536.

Iskander, M., 2020. Stability of the Northern coast of Egypt under the effect of urbanization and climate change. Water Science 35. https://doi.org/10.1080/11104929.2020.1864255.

Khan, S., Wilson, B., Ramsook, R., Vincent, H., 2023. The morphodynamics and sedimentology of a seasonally controlled microtidal tidal inlet: the Nariva River tidal inlet, Cocos Bay, Trinidad. Journal of Sedimentary Research 93, 945–971. https:-//doi.org/10.2110/jsr.2022.041.

Larson, M., Hanson, H., Hamed, Y., Balah, M., Tolba, E., 2007. Impact of coastal erosion and sedimentation along the northern coast of the sinai peninsula. Proceedings of the 8th International Conference on the Mediterranean Coastal Environment, MEDCOAST 2007 2, 1049–1062.

Liu, Y., Wang, Z., Wang, J., Ferrare, R.A., Newsom, R.K., Welton, E.J., 2011. The effect of aerosol vertical profiles on satellite-estimated surface particle sulfate concentrations. Remote Sens Environ 115, 508–513. https://doi.org/10.1016/j.rse.-2010.09.019.

Mandal, S., Chaudhuri, S., 2021. Hydrodynamic stability of tidal inlet system: A case study of Pichaboni inlet, Purba Medinipur, West Bengal, India. Reg Stud Mar Sci 46, 101869. https://doi.org/10.1016/j.rsma.2021.101869.

Mangor, K., Drønen, N.K., Kærgaard, K.H., Kristensen, S.E., 2017. Shoreline management guidelines, DHI Water and Environment.

Mansour, N., Sarhan, T., El-Gamal, M., Nassar, K., 2024. Assessing the compatibility of EPR rates with one-dimensional numerical modelling in monitoring shoreline kinematics along with supplying near/long-term forecasts. Reg Stud Mar Sci 71, 103391. https://doi.org/10.1016/j.rsma.2024.103391.

Mirdan, M.M., Tolba, E.R., Abdellah, S., Galal, E.M., 2023. Digital shoreline analysis system techniques for stability detection: An applied case study on Port Said, Egypt. Egypt J Aquat Res. https://doi.org/10.1016/j.ejar.2023.08.001.

Mohamed, R., Abdalla, D., Abd-El-Mooty, M., 2023. Numerical Modelling for Morphological Changes Along the Nile

Delta Coast (El-Banaieen Area).

Morsy, A., Ebeid, M., Soliman, A., Halim, A.A., Ali, A.E., Fahmy, M., 2022. Evaluation of the water quality and the eutrophication risk in Mediterranean sea area: A case study of the Port Said Harbour, Egypt. Environmental Challenges 7, 100484. https://doi.org/10.1016/j.envc.2022.100484.

Naef, D., Rickenmann, D., Rutschmann, P., W McArdell, B., 2006. Comparison of flow resistance relations for debris flows using a one-dimensional finite element simulation model. Natural Hazards and Earth System Sciences 6, 155–165. https://doi.org/10.5194/nhess-6-155-2006.

Nassar, K., Mahmod, W., Fath, H., Masria, A., Nadaoka, K., Negm, A., 2018a. Shoreline change detection using DSAS technique: Case of North Sinai coast, Egypt. Marine Georesources and Geotechnology 37. https://doi.org/10.1080/1064119X.2018.1448912.

Nassar, K., Mahmod, W., Fath, H., Masria, A., Nadaoka, K., Negm, A., 2018b. Shoreline change detection using DSAS technique: Case of North Sinai coast, Egypt. Marine Georesources and Geotechnology 37. https://doi.org/10.1080/1064119X.2018.1448912.

Nassar, K., Mahmod, W.E., Masria, A., Fath, H., Nadaoka, K., 2018c. Numerical simulation of shoreline responses in the vicinity of the western artificial inlet of the Bardawil Lagoon, Sinai Peninsula, Egypt. Applied Ocean Research 74, 87–101. https://doi.org/10.1016/j.apor.2018.02.015.

Oyedotun, T.D.T., Nedd, G.A., 2023. River mouth morphodynamics and deflection over the short term: effects on spit growth and mangrove dynamics. Front Environ Sci 11, 1–16. https://doi.org/10.3389/fenvs.2023.1181627.

Radwan, A.M., Magdy, M., Rabah, M., Saber, A., Zaki, A., 2021. Sea level analysis using tide gauge observations at the northern delta coast, Egypt. NRIAG Journal of Astronomy and Geophysics 10, 361–371. https://doi.org/10.1080/20909977.2021.1940742.

Redwan, M., Elhaddad, E., 2022. Heavy metal pollution in Manzala Lake sediments, Egypt: sources, variability, and assessment. Environ Monit Assess 194, 436. https://doi.org/10.1007/s10661-022-10081-0.

Saha, D., Rahman, A., Khalifa, A.M., Soliman, M.R., Yassin, A.A., Ari Guner, H.A., Sahin, C., Yuksel, Y., Cevik, E., Noujas, V., Kankara, R.S., Chenthamil Selvan, S., Quang, D.N., Anh, N.Q.D., Tam, H.S., Tinh, N.X., Tanaka, H., Viet, N.T., Rajasree, B.R., Deo, M.C., Khalifa, A.M., Nassar, K., Mahmod, W.E., Masria, A., Fath, H., Nadaoka, K., Sanhory, A., El-Tahan, M., Moghazy, H.M., Reda, W., Sarhan, T.A., Mansour, N., El-Gamal, M., Nassar, K., Elkotby, M.R., Sarhan, T.A., El-Gamal, M., Tharwat Sarhan, A., Mina Iskander, M., Nassar, K., El-Gamal, M., Sarhan, T.A., Mansour, N., El-Gamal, M., Anton, I.A., Panaitescu, M., Panaitescu, F. V., 2017. Assessment of a combination between hard structures and sand nourishment eastern of Damietta harbor using numerical modeling. Alexandria Engineering Journal 56, 545–555. https://doi.org/10.1016/j.aej.2017.04.009.

Salah, H., 2024. Using Machine Learning Techniques to Predict Significant Wave Height Using Machine Learning Techniques to Predict Significant Wave Height Compared with Parametric Methods. https://doi.org/10.11648/j.eas.20240905.12.

Sanhory, A., El-Tahan, M., Moghazy, H.M., Reda, W., 2022. Natural and manmade impact on Rosetta eastern shoreline using satellite Image processing technique. Alexandria Engineering Journal 61, 6247–6260. https://doi.org/10.1016/j.aej.2021.11.053.

Sarhan, A., Masria, A., Ahmed, M., Sharaan, M., Eladawy, A., 2022. Management strategies for Complex Sedimentation process: A Case Study Using Remote Sensing and Morphodynamics Simulation at Damietta Harbor, Nile Delta. International Journal of River Basin Management 22, 1–18. https://doi.org/10.1080/15715124.2022.2101463.

Sarhan, A.T., Iskander, M.M., Nassar, K., Gamal, M. El, 2022. Shoreline Changes Detection Using Digital Shoreline Analysis System: Case Study Damietta – Port Said Coastal Area, Egypt 47.

Sarhan, T., Mansour, N., El-Gamal, M., Nassar, K., 2020. Historical shoreline trend analysis in the vicinity of El-Hammra port at Northwestern coast of Egypt. J Sustain Sci Manag 15, 36–50.

Sarhan, T., Mansour, N., El-gamal, M., Nassar, K., 2020. HISTORICAL SHORELINE TREND ANALYSIS IN THE VICINITY OF EL-HAMMRA PORT AT NORTH WESTERN COAST OF EGYPT 15, 36–50.

Shaltout, M., Tonbol, K., 2011. Modeling of wave propagation off Damietta-Port Said Coast , Egypt. Journal of The Arab Institute of Navigation I, 56–67.

Shaltout, M., Tonbol, K., Omstedt, A., 2015. Sea-level change and projected future flooding along the Egyptian Mediterranean coast. Oceanologia 57, 293–307. https://doi.org/10.1016/j.oceano.2015.06.004.

Subiyanto, S., Supian, S., 2021. Utilizing MIKE 21 Software to Create Simple Hydrodynamic Simulations. International Journal of Research in Community Services 2, 14–17. https://doi.org/10.46336/ijrcs.v2i1.156.

Tharwat Sarhan, A., Mina Iskander, M., Nassar, K., El-Gamal, M., 2022. Shoreline Changes Detection Using Digital Shoreline Analysis System: Case Study Damietta – Port Said Coastal Area, Egypt. MEJ. Mansoura Engineering Journal 47, 35–48. https://doi.org/10.21608/bfemu.2022.236869.

Tolba, E., 2012. Impact of Coastal Erosion and Sedimentation along the Northern Coast of Sinai Peninsula, Case Study: AL-ARISH Harbor Coast. Port-Said Engineering Research Journal 16, 118–125. https://doi.org/10.21608/pserj.2012.103723.